JOURNAL OF CHEMICAL PHYSICS VOLUME 119, NUMBER 23 15 DECEMBER 2003

# Cross-relaxation between macromolecular and solvent spins: The role of long-range dipole couplings

Bertil Halle
*Department of Biophysical Chemistry, Lund University, SE-22100 Lund, Sweden*

(Received 29 August 2003; accepted 22 September 2003)

Nuclear spin relaxation by intermolecular dipole–dipole interactions between macromolecular and solvent nuclear moments forms the basis of a widely used method for investigating macromolecular solvation. In particular, intermolecular cross-relaxation [or nuclear Overhauser effect (NOE)] between protein and water protons has been used to probe the mobility of water molecules interacting with the protein surface. The method rests on the assumption that the intermolecular NOE is of short (4–5 Å) range and thus provides information about the mobility of individual water molecules in hydration sites near the monitored protein protons. Here, we present a theoretical analysis of the spectral density function (SDF) that governs the cross-relaxation rates in the laboratory-fixed and rotating frames. In contrast to the $r^{-6}$ dependence of the intramolecular NOEs used for structure determination, the intermolecular NOE is shown to be long-ranged with important contributions from thousands of water molecules. For a consistent interpretation of such NOEs, it is necessary to use a model that explictly incorporates motionally retarded hydration water molecules as well as unperturbed bulk water molecules. We formulate a diffusion model with a nonuniform solvent mobility and solve it to obtain an analytical expression for the SDF. Calculations with this nonuniform diffusion model demonstrate that intermolecular NOEs with surface protons are dominated by long-range dipole couplings to bulk water and therefore provide little or no information about hydration dynamics. The physical basis of this unexpected phenomenon is that the characteristic time scale for relaxation-inducing fluctuations is longer for the more numerous remote water molecules, despite their higher mobility. The analytical results presented here are generally applicable to intermolecular dipolar relaxation of like or unlike (nuclear or electron) spins in a variety of experimental situations. *© 2003 American Institute of Physics.* [DOI: 10.1063/1.1625632]

## I. INTRODUCTION

The dipolar interaction of nuclear magnetic moments, rendered time-dependent by thermal molecular motions, is the main source of spin relaxation for spin-1/2 nuclides like $^{1}$H, $^{13}$C, and $^{15}$N.[1] Among the various interactions that couple the nuclear spins to the molecular degrees of freedom, the magnetic dipole–dipole interaction is unique in that it can be modulated by both translational and rotational motions. If the dipole-coupled spins belong to the same (rigid) molecule, only the orientation of the internuclear vector can fluctuate and the only relevant molecular motion is rotation. The theoretical treatment of this intramolecular case is relatively straightforward. If the coupled spins belong to different molecules, also the length of the internuclear vector can fluctuate. The treatment of this intermolecular case is more complicated, involving not only the rotation of the two molecules but also their relative translational motion.

In the first theoretical analysis of intermolecular dipolar relaxation, the translational motion was modeled as a random walk on a lattice.[2] For liquids, a continuous diffusion model is more appropriate. To prevent the dipole interaction from diverging, it is then necessary to introduce a distance of closest approach between the two spins. In the first continuum treatment, this was done by introducing a step-function pair correlation function.[1] Subsequently, a fully consistent treatment was presented,[3,4] where the molecular excluded volume was introduced via a reflection boundary condition for the diffusion equation, thereby ensuring that the diffusion propagator evolves towards the correct (step-function) equilibrium pair correlation function. The model was further elaborated by allowing the spins to be located away from the molecular center,[5] in which case also molecular rotation modulates the intermolecular dipole coupling. (Spin eccentricity had previously been taken into account in a less general treatment.[6])

The diffusion theory of intermolecular dipolar relaxation was originally developed with liquids and solutions of small molecules in mind. For such applications, it was of interest to further generalize the model by describing intermolecular forces in a more realistic way than by an excluded volume.[3,7,8] More recently, the theory has been used to interpret the intermolecular nuclear Overhauser effect (NOE) produced by dipolar cross-relaxation between macromolecular and solvent spins. In particular, the interpretation of numerous intermolecular $^{1}$H–$^{1}$H NOE studies of protein hydration rely on the diffusion theory of intermolecular dipolar relaxation.[9–12] The logic underlying the interpretation of water–protein NOEs goes as follows. Because the dipole–dipole coupling decays with the inverse third power of the internuclear separation, the cross-relaxation rate, which involves the square of the dipole coupling, is short-ranged.

0021-9606/2003/119(23)/12372/14/$20.00

Accordingly, intramolecular NOEs are usually observed only for protons separated by less than 4 or 5 Å.[9–12] For the same reason it is generally assumed[9–12] that, although the water $^1$H resonance is due to all water molecules in the sample, the intermolecular NOE is due to only one or a few water molecules near the monitored protein proton.

While the square of the dipole coupling between a protein proton and a water proton at a distance $r$ scales as $r^{-6}$, the number of water protons at a given distance $r$ increases as $r^2$ (ignoring the short-ranged excluded volume effect). Moreover, the characteristic time for modulation of the orientation of the internuclear vector $\mathbf{r}$ by translational diffusion of a water molecule across a given solid angle also increases as $r^2$. The measured cross-relaxation rate, which has contributions from water protons at all separations $r$, is thus obtained by integrating the product $r^{-6}\times r^2 \times r^2 = r^{-2}$ over $r$. Consequently, the zero-frequency spectral density that enters the cross-relaxation rate scales as the inverse of the distance of closest approach,[1] rather than as the inverse sixth power.

In the usual interpretation of protein-water NOEs, the quantity of primary interest is the ratio $\sigma_L/\sigma_R$ of the laboratory-frame and rotating-frame cross-relaxation rates deduced from the measured cross-peak intensities.[9–12] With the aid of the diffusion model[5] and plausible values for several model parameters, the translational diffusion coefficient $D_T$ of the water molecules is extracted. In the final step, a water residence time pertaining to a hydration site near the observed protein proton is calculated from the Einstein–Smoluchowski relation $\tau_{\mathrm{res}} = \delta^2/(6D_T)$, with the root-mean-square displacement $\delta$ taken as 4 Å.[11,12] The validity of this procedure rests on the assumption that the NOE is short-ranged. However, as argued here, this is not the case. Under most conditions, the NOE is thus governed largely by the diffusion of bulk water molecules that are not affected by the protein. Given the long-range nature of the NOE, a consistent interpretation of experimental NOE data in terms of hydration dynamics requires a model that allows the water diffusion coefficient in the hydration layer next to the protein surface to differ from that in the bulk solvent. It is therefore necessary to generalize the diffusion model of intermolecular dipolar relaxation to the case of a solvent with nonuniform mobility.

The derivation of the spectral density function for the nonuniform diffusion model is presented in Sec. II. In the first three subsections, we formulate the model and define the mathematical problem. In the process, we present a novel treatment of translation-rotation decoupling. In the following subsections, we obtain exact analytical solutions of four different versions of the model, including the known case of unrestricted uniform diffusion (Sec. II D). Different boundary conditions are used to examine the range of the intermolecular NOE (Sec. II E) and to model surface accumulation of solvent species such as counterions or cosolvents (Sec. II F). In Sec. II G, we present the spectral density for a solvent with a step-function mobility profile. The results obtained in Sec. II are illustrated in Sec. III by numerical calculations pertaining to cross-relaxation between water and protein protons. In particular, we examine the range of the spectral density and cross-relaxation rates, as well as their dependence on geometrical and dynamic model parameters. We also investigate the interplay of intramolecular and intermolecular NOE contributions, the former arising form buried water molecules or labile protein protons in fast exchange with bulk water. Finally, in Sec. IV, we discuss the implications of the theoretical results for the use of intermolecular NOEs to study macromolecular solvation.

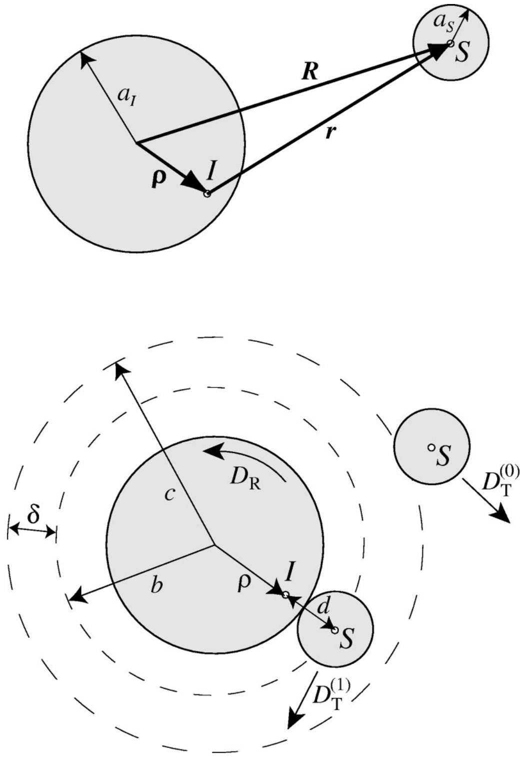

FIG. 1. Definition of model parameters. The parameter $c$ serves both to locate the absorbing (Sec. II E) or reflecting (Sec. II F) boundary and to define the thickness of the solvation shell with perturbed dynamics (Sec. II G).

## II. THEORY

### A. Dynamic model

We consider the spin relaxation induced by magnetic dipole–dipole couplings between a macromolecular spin $I$ and $N_S$ solvent spins $S$ (see Fig. 1). The $I$ spin is located a distance $\rho$ from the center of a spherical macromolecule of radius $a_I$. Each $S$ spin is located at the center of a spherical solvent molecule of radius $a_S$. The distance of closest approach between the centers of the $I$ and $S$ spheres is $b = a_I + a_S$. The $I-S$ internuclear vector $\mathbf{r}$ has a magnitude $r$ that ranges from $d = b - \rho$, the distance of closest approach of the $I$ and $S$ spins, to infinity. Because the $I$ spin is located off-center, the length and orientation of the internuclear vector is modulated by two distinct motions: rotational diffusion of the macromolecule, with rotational diffusion coefficient $D_R$, and translational diffusion of the macromolecule and solvent molecules, with *relative* translational diffusion coefficient $D_T$. In all previous treatments, it has been assumed that $D_T$ is spatially uniform. The essential new element of the present analysis is to allow for a dynamic perturbation of solvent near the macromolecule. We thus stipulate that the relative diffusion coefficient takes the value $D_T^{(1)}$ when the center of the $S$ sphere is within a distance $\delta = c - b$ of the accessible surface of the $I$ sphere and a value $D_T^{(0)}$ elsewhere (see Fig. 1).

Within the motional-narrowing regime,[1] the spin relaxation behavior is fully determined by the rank-2 spectral density function (SDF) $J^{(2)}(\omega)$. In general, the rank-$L$ SDF $J^{(L)}(\omega)$ is the real part of the complex-valued SDF $\mathcal{J}^{(L)}(\omega)$, defined as the Fourier–Laplace transform of the corresponding time autocorrelation function (TCF) $G^{(L)}(\tau)$:

$$\mathcal{J}^{(L)}(\omega) = \int_0^\infty d\tau \exp(-i\omega\tau) G^{(L)}(\tau). \tag{2.1}$$

The TCF for intermolecular dipolar coupling to $N_S$ $S$ spins, whose motions are taken to be uncorrelated, is given by

$$G^{(L)}(\tau) = 4\pi N_S \langle F_{L,0}(\mathbf{r}_0) F_{L,0}(\mathbf{r}) \rangle. \tag{2.2}$$

The angular brackets in Eq. (2.2) signify an ensemble average and $F_{L,0}(\mathbf{r})$ is a rank-$L$ solid harmonic

$$F_{L,0}(\mathbf{r}) = r^{-(L+1)} Y_{L,0}(\Omega), \tag{2.3}$$

where $Y_{L,0}(\Omega)$ is the corresponding spherical harmonic and $\Omega$ denotes the spherical polar angles that specify the orientation of the internuclear vector $\mathbf{r}$ with respect to the laboratory-fixed frame.

### B. Translation-rotation decoupling

The rank-2 TCF of primary interest here can be written

$$G^{(2)}(\tau) = 4\pi N_S \langle F_{2,0}(\mathbf{R}_0 - \boldsymbol{\rho}_0) F_{2,0}(\mathbf{R} - \boldsymbol{\rho}) \rangle. \tag{2.4}$$

The vector $\mathbf{R}$ connecting the centers of the $I$ and $S$ spheres (see Fig. 1) is only modulated by translational diffusion, whereas the offset vector $\boldsymbol{\rho}$, of fixed length $\rho$, is only modulated by rotational diffusion. To an excellent approximation, macromolecular rotation and solvent–macromolecule relative translational diffusion can be treated as statistically independent processes. As shown in the Appendix, the two motions are then decoupled in the sense that the TCF can be expressed as a sum of products of rotational and translational partial TCFs,[5]

$$G^{(2)}(\tau) = \frac{2\pi}{3} \sum_{L=0}^{\infty} (L+1)(L+2)(2L+3)\rho^{2L} \times G_R^{(L)}(\tau) G_T^{(L+2)}(\tau). \tag{2.5}$$

The purely rotational TCF $G_R^{(L)}(\tau)$ is given by Eq. (A5) and the purely translational TCF $G_T^{(L)}(\tau)$ corresponds to the case where also the $I$ spin is located at the center of its sphere,

$$G_T^{(L)}(\tau) = 4\pi N_S \langle F_{L,0}(\mathbf{R}_0) F_{L,0}(\mathbf{R}) \rangle. \tag{2.6}$$

Combination of Eqs. (2.1) and (2.5) yields for the total SDF,

$$\mathcal{J}^{(2)}(\omega) = \mathcal{J}_T^{(2)}(\omega) + \frac{1}{6} \sum_{L=1}^{\infty} (L+1)(L+2) \times (2L+3)\rho^{2L} \mathcal{J}_T^{(L+2)}(\omega_R^{(L)}), \tag{2.7}$$

where $\mathcal{J}_T^{(L)}(\omega)$ is the Fourier–Laplace transform of the translational TCF in Eq. (2.6). The complex-valued frequency $\omega_R^{(L)}$ is defined as

$$\omega_R^{(L)} = \omega - iL(L+1)D_R, \tag{2.8}$$

where $D_R$ is the rotational diffusion coefficient of the macromolecule.

It is straightforward to generalize the model to allow also the $S$ spin to be located off-center.[5] The additional parameter thereby introduced would hardly make the model more realistic. An off-center location of the $S$ spin only affects the TCF on the picosecond time scale of solvent rotation (see Appendix), where the force-free diffusion equation (see below) is not expected to be quantitatively accurate. Here, we focus on the behavior of the TCF on longer time scales.

### C. Diffusion propagator

The ensemble average in Eq. (2.6) can be expressed as

$$G_T^{(L)}(\tau) = 4\pi N_S \int d\mathbf{R}_0 \int d\mathbf{R}\, f(\mathbf{R}_0) \times f(\mathbf{R},\tau|\mathbf{R}_0) F_{L,0}(\mathbf{R}_0) F_{L,0}(\mathbf{R}). \tag{2.9}$$

For a solvent of uniform density, the equilibrium probability density $f(\mathbf{R}_0)$ is $1/V$ for $R_0 \geqslant b$ and zero elsewhere. [For $N_S \gg 1$, the pair correlation function is $g(\mathbf{R}) = V f(\mathbf{R})$.] The propagator $f(\mathbf{R},\tau|\mathbf{R}_0)$ is taken to obey the force-free diffusion equation

$$\frac{\partial}{\partial\tau} f(\mathbf{R},\tau|\mathbf{R}_0) = \nabla \cdot D_T(R) \nabla f(\mathbf{R},\tau|\mathbf{R}_0) \tag{2.10}$$

with the initial condition

$$f(\mathbf{R},0|\mathbf{R}_0) = \delta(\mathbf{R} - \mathbf{R}_0). \tag{2.11}$$

Combination of Eqs. (2.1) and (2.9) yields

$$\mathcal{J}_T^{(L)}(\omega) = 4\pi n_S \int' d\mathbf{R}_0 \int d\mathbf{R}\, f(\mathbf{R},\omega|\mathbf{R}_0) \times F_{L,0}(\mathbf{R}_0) F_{L,0}(\mathbf{R}), \tag{2.12}$$

where $n_S = N_S/V$ is the $S$-spin number density and the prime means that the integration domain excludes the region $R_0 < b$. In Eq. (2.10), $D_T$ is the relative translational diffusion coefficient of the solvent molecules with respect to the macromolecule. In a region of uniform $D_T$, the Fourier–Laplace transformed propagator $f(\mathbf{R},\omega|\mathbf{R}_0)$ satisfies

$$(\nabla^2 - \kappa^2) f(\mathbf{R},\omega|\mathbf{R}_0) = -\delta(\mathbf{R} - \mathbf{R}_0)/D_T \tag{2.13}$$

with

$$\kappa = (i\omega/D_T)^{1/2}. \tag{2.14}$$

The symmetry of the problem requires the general solution to Eq. (2.13) to be of the form

$$f(\mathbf{R},\omega|\mathbf{R}_0) = \sum_{N=0}^{\infty} \rho_N(R|R_0) P_N(\cos\gamma), \tag{2.15}$$

where $P_N(z)$ is a Legendre polynomial, $\gamma$ is the angle between $\mathbf{R}$ and $\mathbf{R}_0$, and $\rho_N(R|R_0)$ is a linear combination of modified spherical Bessel functions:

$$\rho_N(R|R_0)=\alpha_N(R_0)i_N(\kappa R)+\beta_N(R_0)k_N(\kappa R). \tag{2.16}$$

We now substitute Eqs. (2.3) and (2.15) into Eq. (2.12), expand $P_N(\cos\gamma)$ with the aid of the spherical harmonic addition theorem, and use the spherical harmonic orthogonality relation to carry out the angular integrations.[13] The result is

$$\mathcal{J}_T^{(L)}(\omega)=\frac{16\pi^2 n_S}{2L+1}\int_b^\infty dR_0\, R_0^{1-L}\int_b^\infty dR R^{1-L}\rho_L(R|R_0). \tag{2.17}$$

The remaining mathematical problem is to determine the coefficients $\alpha_N(R_0)$ and $\beta_N(R_0)$ in Eq. (2.16) from the boundary conditions on the propagator and, then, to carry out the spatial integrations in Eq. (2.17).

### D. Unrestricted uniform diffusion

Previous treatments have considered the case of an infinite diffusion space with uniform diffusion coefficient $D_T$.[1,3–5] The two boundary conditions are then

$$\frac{\partial}{\partial R}f(\mathbf{R},\tau|\mathbf{R}_0)|_{R=b}=0, \tag{2.18a}$$

$$f(\mathbf{R},\tau|\mathbf{R}_0)|_{R\to\infty}=\text{finite}. \tag{2.18b}$$

On account of the singularity in Eq. (2.13) at $\mathbf{R}=\mathbf{R}_0$, we must treat the cases $R<R_0$ and $R>R_0$ separately. For $R<R_0$, the boundary condition (2.18a) yields

$$\rho_L^{<}(R|R_0)=A_L[k_L'(\kappa b)i_L(\kappa R)-i_L'(\kappa b)k_L(\kappa R)], \tag{2.19a}$$

where $k_L'(\kappa b)=dk_L(z)/dz|_{z=\kappa b}$. For $R>R_0$, the boundary condition (2.18b) yields

$$\rho_L^{>}(R|R_0)=B_L k_L(\kappa R) \tag{2.19b}$$

because $i_L(\kappa R)$ diverges for $R\to\infty$. The Green's function that satisfies Eq. (2.13) has the following properties at $R=R_0$:

$$\rho_L^{<}(R_0|R_0)=\rho_L^{>}(R_0|R_0), \tag{2.20a}$$

$$\frac{\partial}{\partial R}[\rho_L^{<}(R|R_0)-\rho_L^{>}(R|R_0)]|_{R=R_0}=\frac{2L+1}{4\pi R_0^2 D_T}. \tag{2.20b}$$

These two relations determine the coefficients $A_L$ and $B_L$ in Eq. (2.19).

Inserting these results into Eq. (2.17) and performing the integrations (with the integration domain subdivided to avoid the singularity at $R=R_0$), we obtain for $L\geqslant 1$;

$$\mathcal{J}_T^{(L)}(\omega)=\frac{4\pi n_S}{D_T b^{2L-3}}\frac{1}{\zeta^2}\left\{\frac{1}{2L-1}-\frac{(L+1)}{\zeta^2}\times\left[1+\frac{(L+1)}{\zeta}\frac{K_{L+1/2}(\zeta)}{K_{L-1/2}(\zeta)}\right]^{-1}\right\}, \tag{2.21}$$

where $K_\nu(\zeta)$ is a modified Bessel function and

$$\zeta=\kappa b=\left(\frac{i\omega b^2}{D_T}\right)^{1/2}. \tag{2.22}$$

In particular, the rank-2 SDF becomes

$$\mathcal{J}_T^{(2)}(\omega)=\frac{16\pi n_S}{27 D_T b}\left[\frac{1+\frac{1}{4}\zeta}{1+\zeta+\frac{4}{9}\zeta^2+\frac{1}{9}\zeta^3}\right] \tag{2.23}$$

in accord with the known result.[3,4]

### E. Restricted uniform diffusion with absorbing boundary

One of our objectives here is to determine the contribution to the SDF $J^{(2)}(\omega)$ from relatively distant $S$ spins. A convenient way to assess the importance of such long-range dipolar couplings is to introduce an absorbing boundary at a variable radial distance $c$ from the center of the macromolecule (see Fig. 1). In this way, we can isolate the contribution to $J^{(2)}(\omega)$ from solvent spins located in the shell $b\leqslant R\leqslant c$. Mathematically, this is accomplished by replacing Eq. (2.18b) by the absorption boundary condition

$$f(\mathbf{R},\tau|\mathbf{R}_0)|_{R=c}=0. \tag{2.24}$$

Furthermore, the equilibrium probability density $f(\mathbf{R}_0)$ is now $1/V$ for $b\leqslant R_0\leqslant c$ and zero elsewhere. This simply means that the upper integration limit for $R_0$ and $R$ in Eq. (2.17) now is $c$ rather than infinity. The boundary condition (2.24) is satisfied by

$$\rho_L^{>}(R|R_0)=B_L[k_L(\kappa c)i_L(\kappa R)-i_L(\kappa c)k_L(\kappa R)]. \tag{2.25}$$

The coefficients $A_L$ in Eq. (2.19a) and $B_L$ in Eq. (2.25) are determined by the matching conditions (2.20).

Proceeding as in the unrestricted case, we obtain from Eq. (2.17),

$$\mathcal{J}_T^{(L)}(\omega)=\frac{4\pi n_S}{D_T b^{2L-3}}\frac{1}{\zeta^2}\left(\frac{1-\lambda^{2L-1}}{2L-1}-\frac{(L+1)(1+\lambda^{2L+1})}{\zeta^2}+\frac{1}{Q_L(i'k)}\left\{\frac{2(L+1)\lambda^{L+1}}{\zeta^4}-\frac{(L+1)^2}{\zeta^3}Q_L(ik)-\frac{\lambda^{2L}}{\zeta}Q_L(i'k')\right\}\right) \tag{2.26}$$

with

$$Q_L(ik)=i_L(\zeta)k_L(\zeta/\lambda)-k_L(\zeta)i_L(\zeta/\lambda), \tag{2.27a}$$

$$Q_L(i'k)=i_L'(\zeta)k_L(\zeta/\lambda)-k_L'(\zeta)i_L(\zeta/\lambda), \tag{2.27b}$$

$$Q_L(i'k')=i_L'(\zeta)k_L'(\zeta/\lambda)-k_L'(\zeta)i_L'(\zeta/\lambda), \tag{2.27c}$$

and

$$\lambda=b/c. \tag{2.28}$$

In the limit $c \rightarrow \infty$, Eq. (2.26) reduces to Eq. (2.21), as required. In the limit $c \rightarrow b$, we have $Q_L = \zeta^{-2}$ and $\mathcal{J}_T^{(L)}(\omega) = 0$, as expected. For $L = 2$, Eq. (2.26) yields in the zero-frequency limit,

$$J_T^{(2)}(0) = \frac{16\pi n_S}{27 D_T b}\left[1 - \frac{\lambda(81 - 30\lambda^2 + 5\lambda^4 + 24\lambda^5)}{16(3 + 2\lambda^5)}\right]. \tag{2.29}$$

### F. Restricted uniform diffusion with reflecting boundary

Throughout this work, we consider only force-free translational diffusion and, by implication, a spatially uniform distribution of solvent molecules. This description may not be appropriate for $S$ spins belonging to one of the components of a binary (or multicomponent) solvent, for example, counterions of a highly charged macromolecule or cosolvent molecules that accumulate at the macromolecular surface. In such cases, the force-free diffusion equation should be replaced by a Smoluchowski equation with a drift term involving the mean force acting on the spin-bearing solvent molecules. In general, this can only be done numerically, e.g., using a finite-difference approach.[3,14] If most of the $S$ spins are confined to the surface region, a somewhat crude, but analytical, description is obtained by imposing a reflecting boundary at a distance $c$ from the center of the macromolecule. The $S$ spins are thus confined to a surface layer of thickness $c - b$.

The treatment for this case closely parallels that in Sec. II E, except that the second boundary condition now reads

$$\frac{\partial}{\partial R} f(\mathbf{R}, \tau | \mathbf{R}_0)|_{R=c} = 0. \tag{2.30}$$

This condition is satisfied by

$$\rho_L^{>}(R|R_0) = B_L[k_L'(\kappa c) i_L(\kappa R) - i_L'(\kappa c) k_L(\kappa R)]. \tag{2.31}$$

The coefficients $A_L$ in Eq. (2.19a) and $B_L$ in Eq. (2.31) are determined by the matching conditions (2.20) as before. Noting that the $S$ spin number density now depends on $c$ according to $n_S = 3N_S/[4\pi(c^3 - b^3)]$, we obtain with Eq. (2.17),

$$\begin{aligned}\mathcal{J}_T^{(L)}(\omega) = \frac{3N_S}{D_T b^{2L}(\lambda^{-3} - 1)} \frac{1}{\zeta^2} \Bigg( &\frac{1 - \lambda^{2L-1}}{2L - 1} \\ &- \frac{(L+1)(1 - \lambda^{2L+1})}{\zeta^2} - \frac{(L+1)^2}{\zeta^3 Q_L(i'k')} \\ &\times \left\{ Q_L(ik') + \lambda^{2L+2} Q_L(k'i) + \frac{2\lambda^{L+2}}{\zeta^2} \right\} \Bigg),\end{aligned} \tag{2.32}$$

with $\lambda$ and $Q_L(i'k')$ as defined in Sec. II E, and

$$Q_L(ik') = i_L(\zeta) k_L'(\zeta/\lambda) - k_L(\zeta) i_L'(\zeta/\lambda), \tag{2.33a}$$

$$Q_L(k'i) = k_L'(\zeta) i_L(\zeta/\lambda) - i_L'(\zeta) k_L(\zeta/\lambda). \tag{2.33b}$$

In the limit $c \rightarrow \infty$, Eq. (2.32) reduces to Eq. (2.21), as required. In the limit $c \rightarrow b$, the real part of Eq. (2.32) yields the rank-$L$ SDF for surface diffusion on a sphere,[15]

$$J_T^{(L)}(\omega) = \frac{N_S}{b^{2L+2}} \frac{\tau_{\mathrm{sd}}^{(L)}}{1 + (\omega \tau_{\mathrm{sd}}^{(L)})^2} \tag{2.34}$$

with the rank-$L$ surface-diffusion correlation time $\tau_{\mathrm{sd}}^{(L)} = b^2/[L(L+1)D_T]$.

### G. Unrestricted nonuniform diffusion

An important motivation for the present work is the need for a consistent theoretical treatment of dynamic solvation effects in the context of intermolecular dipolar spin relaxation. To this end, we generalize the dynamic model used in Secs. II D–II F by allowing the relative translational diffusion coefficient to take different values in a ‘‘solvation layer’’ of thickness $c - b$ and in the ‘‘bulk’’ solvent. We thus stipulate that

$$D_T = \begin{cases} D_T^{(1)}, & b \leqslant R < c \\ D_T^{(0)}, & R \geqslant c. \end{cases} \tag{2.35}$$

The Fourier–Laplace transformed propagator is obtained by solving Eq. (2.13) separately for each homogeneous region and then matching the resulting propagators $f^{(0)}(\mathbf{R}, \omega | \mathbf{R}_0)$ and $f^{(1)}(\mathbf{R}, \omega | \mathbf{R}_0)$ by requiring that they and the associated fluxes vary continuously across the surface $R = c$.[14] We thus impose the continuity conditions

$$\rho_L^{(1)}(c|R_0) = \rho_L^{(0)}(c|R_0), \tag{2.36a}$$

$$D_T^{(1)} \frac{\partial}{\partial R} \rho_L^{(1)}(R|R_0)|_{R=c} = D_T^{(0)} \frac{\partial}{\partial R} \rho_L^{(0)}(R|R_0)|_{R=c}. \tag{2.36b}$$

For each of the two propagators, we must investigate separately the cases where $R_0$ is $< c$ or $> c$ and where $R_0$ is $< R$ or $> R$. Altogether, we must therefore determine the expansion coefficients in Eq. (2.16) in six cases. After a lengthy calculation, we obtain from Eq. (2.17),

$$\begin{aligned}\mathcal{J}_T^{(L)}(\omega) = \frac{4\pi n_S}{D_T^{(0)} b^{2L-3}} \frac{1}{\zeta_0^2} \Bigg( &\frac{1}{2L - 1} + \lambda^{L-1} \zeta_1 Q_{L-1}(ik) \\ &- \frac{1}{T_L^k} \Bigg\{ \lambda^{2L-2} \zeta_0 k_{L-1}(\zeta_0/\lambda) X_L \\ &+ \left[ \zeta_1 Y_L - \frac{2\lambda^{L+1}}{\zeta_0} k_{L-1}(\zeta_0/\lambda) \right] V_L \Bigg\} \Bigg),\end{aligned} \tag{2.37}$$

where we have introduced the following auxilliary quantities:

$$\begin{aligned} Q_{L-1}(ik) = {} & i_{L-1}(\zeta_1) k_{L-1}(\zeta_1/\lambda) \\ & - k_{L-1}(\zeta_1) i_{L-1}(\zeta_1/\lambda), \end{aligned} \tag{2.38a}$$

$$S_L^{kk} = \gamma k_L'(\zeta_0/\lambda) k_L(\zeta_1/\lambda) - k_L(\zeta_0/\lambda) k_L'(\zeta_1/\lambda), \tag{2.38b}$$

$$S_L^{ki} = \gamma k_L'(\zeta_0/\lambda) i_L(\zeta_1/\lambda) - k_L(\zeta_0/\lambda) i_L'(\zeta_1/\lambda), \tag{2.38c}$$

$$S_L^{ik} = \gamma i_L'(\zeta_0/\lambda) k_L(\zeta_1/\lambda) - i_L(\zeta_0/\lambda) k_L'(\zeta_1/\lambda), \tag{2.38d}$$

$$S_L^{ii}=\gamma i_L'(\zeta_0/\lambda)i_L(\zeta_1/\lambda)-i_L(\zeta_0/\lambda)i_L'(\zeta_1/\lambda), \tag{2.38e}$$

$$T_L^k=k_L'(\zeta_1)S_L^{ki}-i_L'(\zeta_1)S_L^{kk}, \tag{2.38f}$$

$$T_L^i=k_L'(\zeta_1)S_L^{ii}-i_L'(\zeta_1)S_L^{ik}, \tag{2.38g}$$

$$U_{L-1}^k=k_{L-1}(\zeta_1)-\lambda^{L-1}k_{L-1}(\zeta_1/\lambda), \tag{2.38h}$$

$$U_{L-1}^i=i_{L-1}(\zeta_1)-\lambda^{L-1}i_{L-1}(\zeta_1/\lambda), \tag{2.38i}$$

$$V_L=k_L'(\zeta_1)U_{L-1}^i+i_L'(\zeta_1)U_{L-1}^k, \tag{2.38j}$$

$$X_L=i_{L-1}(\zeta_0/\lambda)T_L^k+k_{L-1}(\zeta_0/\lambda)T_L^i, \tag{2.38k}$$

$$Y_L=S_L^{kk}U_{L-1}^i+S_L^{ki}U_{L-1}^k. \tag{2.38l}$$

The quantities $\zeta_0$ and $\zeta_1$ are defined as in Eq. (2.22), but with $D_T$ replaced by either of the diffusion coefficients in Eq. (2.35). Finally, $\lambda=b/c$ as before and

$$\gamma=[D_T^{(0)}/D_T^{(1)}]^{1/2}. \tag{2.39}$$

In the special case $D_T^{(0)}=D_T^{(1)}$, Eq. (2.37) reduces correctly to Eq. (2.21).

## III. CALCULATIONS

In this section, we use the theoretical results of Sec. II to calculate the rank-2 SDF and the cross-relaxation rates that can be determined from nuclear Overhauser effect (NOE) experiments.[16] To facilitate comparison with experimental results, all calculated SDFs have been multiplied by the dipolar coupling constant

$$K_{IS}=\left(\frac{\mu_0}{4\pi}\hbar\gamma_I\gamma_S\right)^2. \tag{3.1}$$

Here, $\gamma_I$ and $\gamma_S$ are the magnetogyric ratios of the two nuclides and $\mu_0$ is the vacuum permeability. All calculations refer to the homonuclear $^1$H–$^1$H case, with $\gamma_I=\gamma_S=2.675\times10^8\ \mathrm{rad\,(T\,s)^{-1}}$.

The cross-relaxation rates measured in the laboratory (Zeeman) and the rotating (spin-locked) frames are related to the rank-2 SDF as[16]

$$\sigma_L=K_{IS}[0.6\ J^{(2)}(\omega_I+\omega_S)-0.1\ J^{(2)}(\omega_I-\omega_S)], \tag{3.2a}$$

$$\sigma_R=K_{IS}[0.3\ J^{(2)}(\omega_I)+0.2\ J^{(2)}(\omega_I-\omega_S)], \tag{3.2b}$$

where $\omega_I$ and $\omega_S$ are the angular Larmor frequencies of the two spins. In the homonuclear case, $\omega_I=\omega_S=2\pi\nu_0$. Unless otherwise noted, the model parameters have been assigned the values given in Table I, which are representative for a solvent-exposed $^1$H spin in a small protein in water at room temperature, investigated by $^1$H–$^1$H NOE measurements at a $^1$H resonance frequency of 600 MHz.

For reference, we recall that the SDF for an isolated spin pair $I$–$S$ with internuclear vector $\mathbf{r}$ of fixed length $r$ and tumbling isotropically with rank-2 rotational correlation time $\tau_R$ is[1]

$$J^{(2)}(\omega)=\frac{1}{r^6}\,\frac{\tau_R}{1+(\omega\tau_R)^2}. \tag{3.3}$$

This case is commonly referred to as intramolecular dipolar relaxation. For a strong $^1$H–$^1$H dipole coupling, with $r=3$ Å and $\tau_R=7$ ns, Eqs. (3.2) and (3.3) yield $K_{IS}J(0)=5.47\ \mathrm{s}^{-1}$, $\sigma_L=-0.546\ \mathrm{s}^{-1}$, and $\sigma_R=1.10\ \mathrm{s}^{-1}$. The ratio of the intramolecular cross-relaxation rates is $\sigma_L/\sigma_R=-0.498$, close to the slow-motion limit of $-1/2$. In the opposite, fast-motion or extreme-narrowing, limit, $\sigma_L/\sigma_R=1$.

TABLE I. Default parameter values used in calculations.

| Parameter | Symbol | Value | Units |
|---|---|---|---|
| Solvent spin number density[a] | $n_S$ | 2/30 | Å$^{-3}$ |
| Solvent-accessible solute radius | $b$ | 15 | Å |
| Distance of closest $I$–$S$ approach | $d$ | 3 | Å |
| Thickness of solvation layer | $\delta$ | 3 | Å |
| Bulk solvent diffusion coefficient[b] | $D_T^{(0)}$ | $2\times10^{-9}$ | $\mathrm{m^2\,s^{-1}}$ |
| Dynamic perturbation in solvation layer | $D_T^{(0)}/D_T^{(1)}$ | 5 | ⋯ |
| Solute rotational correlation time[c] | $\tau_R$ | 7 | ns |
| Larmor frequency | $\nu_0$ | 600 | MHz |
| Dipolar coupling constant[d] | $K_{IS}$ | $5.7\times10^{11}$ | Å$^6$ s$^{-2}$ |

[a] Proton density in water at 20 °C.

[b] For water at 20 °C.

[c] Estimated for a globular macromolecule of radius $b$ in water at 20 °C.

[d] For two protons.

### A. Uniform diffusion

Because of the $r^{-6}$ dependence in Eq. (3.3), the intramolecular NOE is short-ranged: if the $I$ spin couples to several $S$ spins in the same molecule, the NOE tends to be dominated by the nearest $S$ spin. The case of an intermolecular NOE between a macromolecular spin $I$ and many solvent spins $S$ is qualitatively different in two ways. First, the high uniform density of solvent spins effectively extends to infinity. While distant $S$ spins are only weakly coupled to the $I$ spin, the number of $S$ spins at a given distance $r$ increases as $r^2$. The distance-dependent factor $r^{-6}$ in Eq. (3.3) is thereby changed to $r^{-4}$. Second, in contrast to the intramolecular case, the orientational randomization of different $\mathbf{r}$ vectors takes place on different time scales. Qualitatively, the relevant time scale is given by the correlation time for surface diffusion on a sphere of radius $r$. As noted below Eq. (2.34), this correlation time is proportional to $r^2$. The total contribution to the zero-frequency SDF $J^{(2)}(0)$ from $I$–$S$ spin pairs at different separations $r$ is therefore obtained, not by summing $r^{-6}$ terms, but by integrating $r^{-6}\times r^2\times r^2=r^{-2}$. As a result, the intermolecular NOE, which involves $J^{(2)}(0)$, becomes long-ranged.

The effect of long-range dipole couplings on the SDF can be examined quantitatively by the mathematical device of imposing an absorbing boundary at a variable distance $c$ from the center of the $I$ sphere. In this way, we can isolate the contribution to the SDF from $S$ spins located within a spherical shell extending a distance $\delta=c-b$ out from the solvent-accessible surface of the macromolecule (see Fig. 1). The solid curve in Fig. 2 is the SDF with contributions from all solvent spins included, while the dashed curves are obtained if we only include solvent spins within a shell of the indicated thickness $\delta$. At high frequencies, where the SDF only samples fast motions, slowly modulated long-range dipole couplings do not contribute much. However, even at 1.2

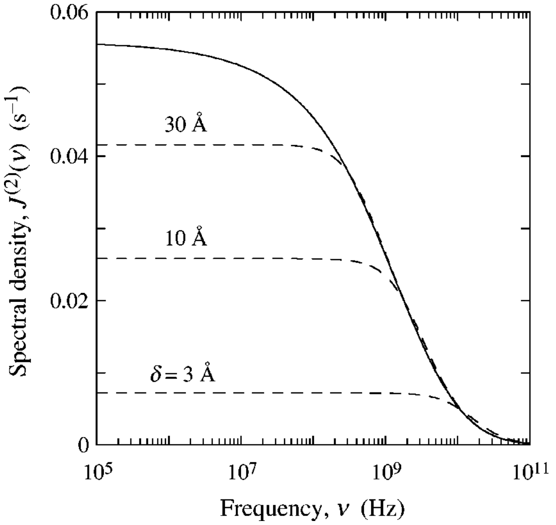

FIG. 2. Spectral density function $J^{(2)}(\nu)$ for unrestricted uniform diffusion with parameter values from Table I (solid curve) and with an absorbing boundary 3, 10, or 30 Å outside the accessible surface of the macromolecule (dashed curves).

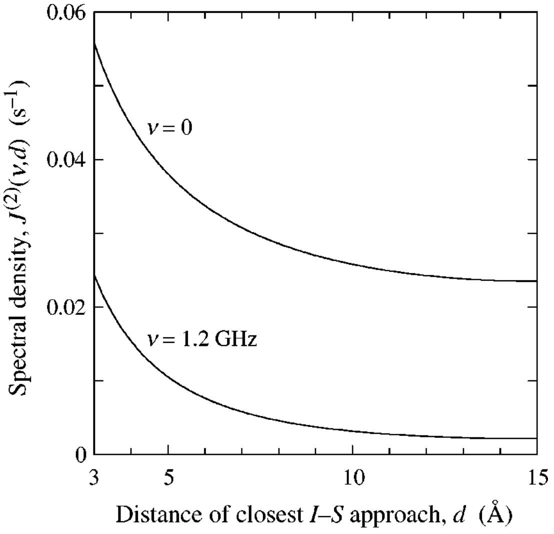

FIG. 4. Spectral density $J^{(2)}(\nu;d)$ at $\nu = 0$ and $\nu = 2 \times 600$ MHz vs the distance of closest approach $d = b - \rho$ between the $I$ spin and an $S$ spin. Unrestricted uniform diffusion with parameter values from Table I.

GHz [the frequency sampled by $J^{(2)}(2\omega_0)$ in a 600 MHz NOE experiment], solvent spins 10 Å from the surface contribute significantly. More importantly, the zero-frequency spectral density $J^{(2)}(0)$ has substantial contributions from solvent spins well beyond 30 Å. This is in contrast to the generally held view[11,12] that only water molecules in the first hydration layer ($\delta \approx 3$ Å) contribute significantly to the NOE.

The convergence of the SDF as more distant solvent spins are included is shown in Fig. 3 at zero frequency and at 1.2 GHz. In the inset, the same SDFs are plotted against the number $N_W$ of contributing water molecules, obtained from $\delta$ with the aid of the geometric relation

$$N_W V_W = \frac{4\pi}{3}[(b+\delta)^3 - b^3], \tag{3.4}$$

where $V_W = 30$ Å$^3$ is the volume occupied by one water molecule. It is seen that $J^{(2)}(0)$ has reached only half of the converged value when 2 000 water molecules are included and that 200 000 water molecules are required for 90% convergence. The asymptotic convergence of $J^{(2)}(0)$ is slow: $N_W^{-1/3}$. Because of the eccentric location of the $I$ spin, all $S$ spins at a given distance from the surface will not make the same contribution to the SDF. However, because the macromolecular radius is only 15 Å, the asymptotic (large $N_W$) behavior of $J^{(2)}(0)$ would hardly be affected if the spherical absorbing boundary were centered on the $I$ spin.

Figure 4 illustrates the dependence of the SDF on the distance of closest approach, $d = b - \rho$, between the $I$ spin and an $S$ spin (see Fig. 1). For water at the surface of a biomolecule, $d$ is rarely less than 3 Å. The maximum value is $d = b = 15$ Å, corresponding to a centered $I$ spin. In the intramolecular case, Eq. (3.3), this range of internuclear separations corresponds to a factor $(15/3)^6 = 15\,625$ variation of the SDF. In the intermolecular case shown in Fig. 4, however, the SDF only varies by factor 2.4 (at zero frequency) or 11 (at 1.2 GHz). This is another manifestation of the long-range nature of the intermolecular SDF, where the few $S$ spins with $r \approx d$ contribute less than the numerous more distant $S$ spins.

In Fig. 5, we examine the dependence of the SDF on the rank-2 rotational correlation time $\tau_R = 6(D_R)^{-1}$ of the macromolecule. The default value $\tau_R = 7$ ns, used in all other figures, is seen to be close to the static limit. Unless the macromolecule is much smaller (like an oligopeptide) or solvent diffusion is much slower (as for water molecules trapped in deep surface pockets), the intermolecular SDF is hardly affected by the rotation of the macromolecule. Also the translational motion of the macromolecule is unimportant. The relative translational diffusion coefficient $D_T$ is the sum of the macromolecular and solvent diffusion coeffi-

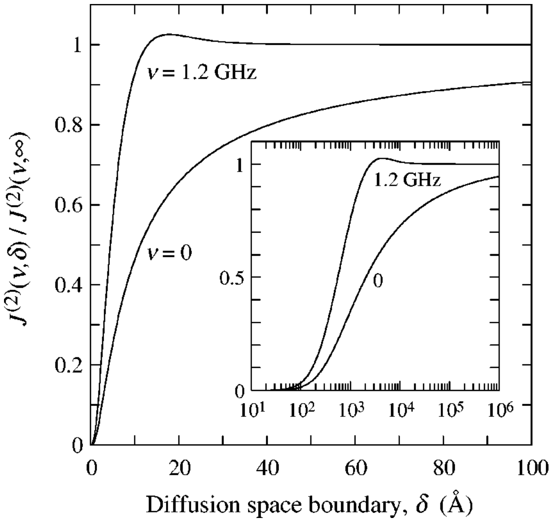

FIG. 3. Relative spectral density $J^{(2)}(\nu;\delta)/J^{(2)}(\nu;\infty)$ at $\nu = 0$ and $\nu = 2 \times 600$ MHz vs the position of an absorbing boundary, at a distance $\delta$ outside the accessible surface of the macromolecule. Unrestricted uniform diffusion with parameter values from Table I. The inset shows the same relative spectral densities vs the number of water molecules inside the diffusion space boundary at $c = b + \delta$.

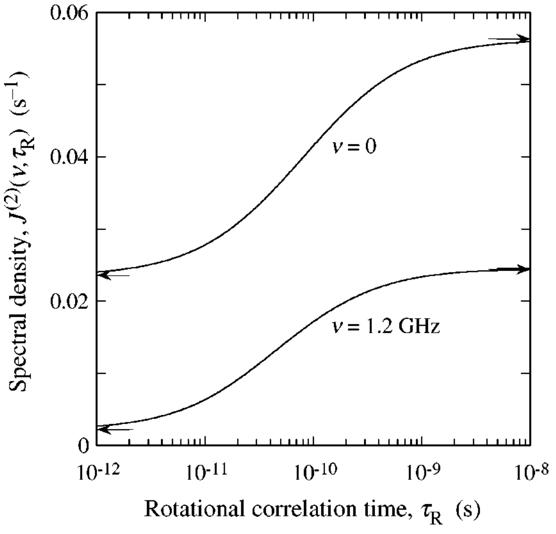

FIG. 5. Spectral density $J^{(2)}(\nu;\tau_R)$ at $\nu=0$ and $\nu=2\times600$ MHz vs the rank-2 rotational correlation time $\tau_R$. Unrestricted uniform diffusion with parameter values from Table I. The arrows correspond to the case of a centered $I$ spin (left) and to the static ($D_R=0$) limit (right).

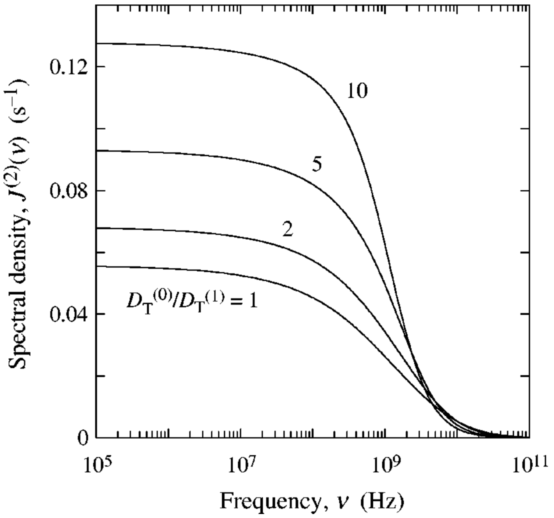

FIG. 6. Spectral density function $J^{(2)}(\nu)$ for unrestricted nonuniform diffusion. Parameter values from Table I and the translational mobility in the solvation layer retarded by a factor 1, 2, 5 or 10.

cients, but for $b \geqslant 15$ Å the former contributes less than 10%. In the limit of very fast macromolecular rotation (short $\tau_R$), the $I$ spin eccentricity is averaged out and the SDF approaches the value calculated with a centered $I$ spin (see Fig. 5). For this reason, our neglect of $S$ spin eccentricity has virtually no effect on the SDF at the frequencies of interest (see Appendix).

### B. Nonuniform diffusion

Close to the macromolecular surface, solvent diffusion is expected to be slower than in the bulk.[17] This dynamic perturbation is short-ranged, essentially confined to the first layer of solvent molecules. We model this effect by assigning a diffusion coefficient $D_T^{(1)}$, lower than the bulk value $D_T^{(0)}$, to $S$ spins located in a surface layer of thickness $\delta=3$ Å. As seen from Fig. 6, such dynamic solvation effects are not strongly manifested in the SDF. Even a tenfold retardation only doubles $J^{(2)}(0)$. For the vast majority of water molecules at a macromolecular surface, we expect that $D_T^{(0)}/D_T^{(1)} \approx 2$ (Refs. 17, 18) and the effect on the SDF is then merely 20%.

In intermolecular NOE studies of biomolecular hydration, information about hydration dynamics is usually deduced from the ratio $\sigma_L/\sigma_R$ of the two cross-relaxation rates. Figure 7 shows that the dynamic solvation effect on this ratio is even smaller than on the SDF. Ironically, $\sigma_L/\sigma_R$ is particularly insensitive to solvation dynamics at the Larmor frequencies used in most intermolecular NOE studies. At 600 MHz, a tenfold retardation of solvent dynamics at the macromolecular surface only reduces $\sigma_L/\sigma_R$ from 0.438 to 0.395, a variation that is smaller than the typical experimental error. At 500 MHz, the corresponding variation is even smaller: from 0.482 to 0.474. Note that these variations are in the opposite direction from what one might expect by analogy with intramolecular NOEs. The reason for the insensitivity of $\sigma_L/\sigma_R$ to dynamics in the solvation layer is that the cross-relaxation rates are dominated by long-range dipole couplings to more distant solvent spins, as demonstrated by the dashed curve in Fig. 7.

Figure 8 shows that the remarkable insensitivity of the ratio $\sigma_L/\sigma_R$ to the mobility of water molecules in the first hydration layer persists for all relevant values of the distance of closest approach, $d$. (In Fig. 7, we used $d=3$ Å.) Only when the translational retardation factor $D_T^{(0)}/D_T^{(1)}$ exceeds 10 does $\sigma_L/\sigma_R$ decrease significantly. Whereas $\sigma_L/\sigma_R$ is insensitive to solvation dynamics, Fig. 8 shows that it depends more strongly on solvent accessibility, modeled here by the distance of closest approach. In fact, $\sigma_L/\sigma_R$ is an order of magnitude more sensitive to $d$ variations in the range 2.5–7.5 Å than to $D_T^{(0)}/D_T^{(1)}$ variations in the range

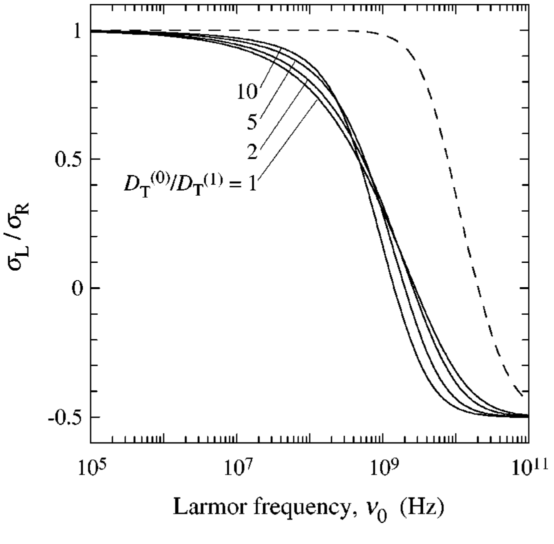

FIG. 7. Ratio of the homonuclear laboratory-frame ($\sigma_L$) and rotating-frame ($\sigma_R$) cross-relaxation rates vs the Larmor frequency. Unrestricted nonuniform diffusion with parameter values from Table I and the translational mobility in the solvation layer retarded by a factor 1, 2, 5 or 10. The dashed curve corresponds to uniform diffusion with an absorbing boundary 3 Å outside the accessible surface of the macromolecule.

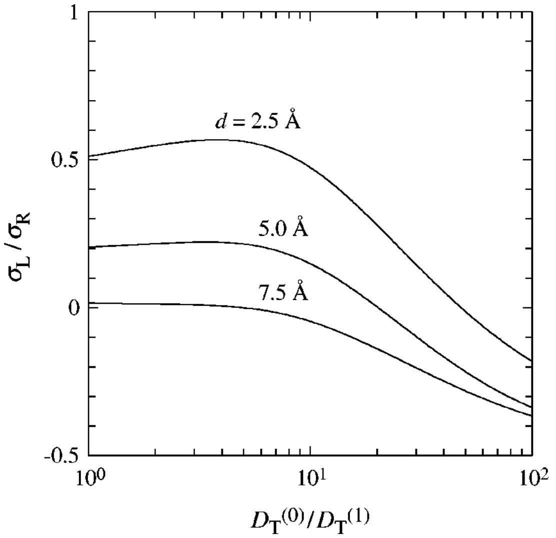

FIG. 8. Ratio of the homonuclear laboratory-frame ($\sigma_L$) and rotating-frame ($\sigma_R$) cross-relaxation rates vs the translational retardation factor $D_T^{(0)}/D_T^{(1)}$. Unrestricted nonuniform diffusion with parameter values from Table I and the indicated distance of closest approach *d*.

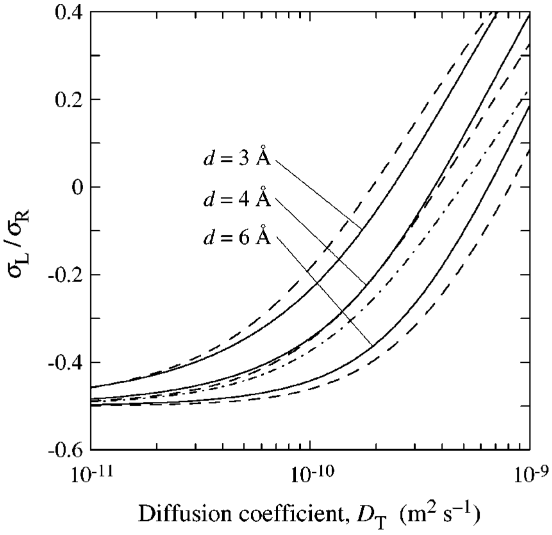

FIG. 9. Ratio of the homonuclear laboratory-frame ($\sigma_L$) and rotating-frame ($\sigma_R$) cross-relaxation rates vs the translational diffusion coefficient $D_T$. Restricted uniform diffusion within a layer of thickness $\delta = 3$ Å (reflecting outer boundary), distance of closest approach $d = 3$, 4 or 6 Å, and other parameter values from Table I. The dashed curve for each *d* value refers to the surface diffusion limit. The dashed–dotted curve corresponds to $d = 4$ Å and layer thickness $\delta = 10$ Å.

1–10. The *d* dependence in Fig. 8 contrasts with the intramolecular case, where the strong $d^{-6}$ dependence of $\sigma_L$ and $\sigma_R$ cancels out in the ratio. The dependence of $\sigma_L$ and $\sigma_R$ (and their ratio) on the distance of closest approach has been investigated previously by calculations based on the uniform diffusion model (with centered spins) and a model with a planar surface (and truncation of the aqueous region at 7 Å).[19]

If the molecular species carrying the *S* spins are strongly attracted by the macromolecular surface, virtually all *S* spins will be found in a surface layer of thickness $\delta$. There are then no long-range dipole couplings that can obscure the effect of solvation dynamics. This situation can be modeled by an outer reflecting boundary a distance $\delta$ outside the solvent-accessible macromolecular surface. As expected, Fig. 9 reveals a pronounced dynamic solvation effect on $\sigma_L / \sigma_R$, along with a considerable accessibility effect (*d* dependence). The difference between confinement to a 3 Å layer and true surface diffusion ($\delta \rightarrow 0$) is seen to be small (dashed curves). Even a 10 Å layer does not deviate much from the surface diffusion limit. The ratio $\sigma_L / \sigma_R$ is sensitive to solvation dynamics only when surface diffusion is fast enough to compete with rotational diffusion, i.e., when $\tau_{\mathrm{sd}}^{(2)} = b^2/(6 D_T) < \tau_R$. For the parameter values used in Fig. 9, this means $D_T > 5 \times 10^{-11}\ \mathrm{m}^2\ \mathrm{s}^{-1}$. The surface diffusion limit should be applicable to counterions and certain cosolvents that accumulate strongly at the macromolecular surface without long-lived association at specific binding sites.

## C. Long-lived association

Up to now, we have considered dipole couplings between a macromolecular *I* spin and a large number $N_S$ of *S* spins in solvent molecules undergoing force-free translational diffusion. In addition to these mobile solvent species, a smaller number $N_M$ of *S* spins may reside at specific macromolecular sites. Even if these specifically bound *S* spins exchange with the pool of mobile *S* spins at a sufficient rate to contribute to the observed *S* resonance, they may experience a substantial exchange barrier. The translational motion of such species is better described by a discrete exchange model than by a force-free diffusion equation. In the case where the mobile *S* spins are water protons, the specifically bound *S* spins may be of three kinds: (1) labile macromolecular protons, such as carboxyl, hydroxyl, ammonium or guandinium protons in amino acid side-chains; (2) protons belonging to internal water molecules trapped in cavities within the macromolecule; and (3) protons in water molecules located in pockets on the macromolecular surface. The two first classes of protons generally have residence times much longer than the rotational correlation time $\tau_R$ of the macromolecule and therefore constitute efficient relaxation sinks.[17,20,21] The third class of protons typically have residence times of order $10^{-10}$ *s*.[17,20,21]

In the presence of freely diffusing as well as specifically bound *S* spins, the SDF can be calculated as the real part of

$$\mathcal{J}^{(2)}(\omega) = \mathcal{J}^{(2)}_{\mathrm{mobile}}(\omega) + \sum_{k=1}^{N_M} \frac{1}{r_k^6} \frac{\tau_{C,k}}{1 + i\omega\tau_{C,k}}. \tag{3.5}$$

The first term, due to mobile *S* spins, is calculated as described in Sec. II. The second term is a sum over all $N_M$ specifically bound *S* spins with $I-S$ internuclear vectors $\mathbf{r}_k$. These are treated as intramolecular dipole couplings, just as in Eq. (3.3), but with the difference that translational motion (exchange with mobile *S* spins) is incorporated via the correlation time $\tau_{C,k}$, determined by the rotational correlation time $\tau_R$ and the mean residence time $\tau_{M,k}$ through[20]

$$\frac{1}{\tau_{C,k}} = \frac{1}{\tau_R} + \frac{1}{\tau_{M,k}}. \tag{3.6}$$

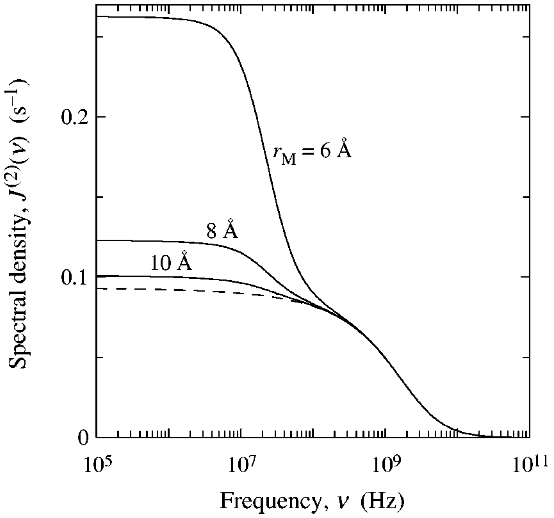

FIG. 10. Spectral density function $J^{(2)}(\nu)$ for unrestricted nonuniform diffusion in the presence of two long-lived ($\tau_M \gg \tau_R$) $S$ spins at a distance $r_M$ from the $I$ spin. Parameter values from Table I. The dashed curve is obtained in the absence of long-lived $S$ spins.

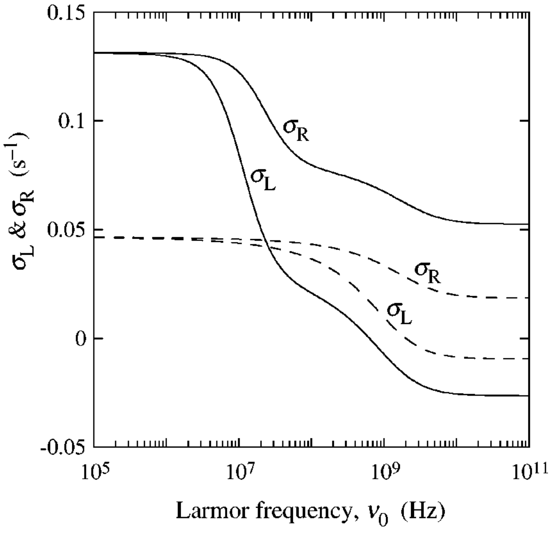

FIG. 11. Homonuclear laboratory-frame ($\sigma_L$) and rotating-frame ($\sigma_R$) cross-relaxation rates vs the Larmor frequency. Unrestricted nonuniform diffusion in the presence of two long-lived $S$ spins at a distance $r_M = 6$ Å from the $I$ spin. Parameter values from Table I. The dashed curves are obtained in the absence of long-lived $S$ spins.

This simple treatment of specifically bound $S$ spins is valid provided that we can neglect the effects of dynamic cross-correlations among different $\mathbf{r}_k$ vectors as well as any internal motions of these vectors.[20] Furthermore, we have assumed that $N_M \ll N_S$.

Figure 10 shows the effect on the SDF of two long-lived ($\tau_M \gg \tau_R$) $S$ spins at a distance $r_M$ of 6, 8 or 10 Å from the $I$ spin, in addition to a large (effectively infinite) number of freely mobile $S$ spins with a five-fold dynamic retardation in the hydration layer ($\delta = 3$ Å). These two long-lived $S$ spins might represent a water molecule buried in an internal cavity or two macromolecular hydroxyl protons. In addition to the broad dispersion centered near 1 GHz, due to translational diffusion of mobile $S$ spins, there is now also a Lorentzian dispersion centered at 20 MHz, reflecting macromolecular tumbling. The low-field dispersion does not affect the spectral densities $J^{(2)}(\omega_0)$ and $J^{(2)}(2\omega_0)$, which typically are dominated by motional frequencies in the GHz range. However, the zero-frequency spectral density $J^{(2)}(0)$ is strongly affected by even a small number of relatively remote, but long-lived, $S$ spins.

In intermolecular NOE studies of protein hydration, it is customary to neglect the effect of labile protons further than 4 Å from the observed $I$ spin.[9,10] Figure 11 shows that this convention is inappropriate. Even two long-lived protons 6 Å from the $I$ spin has a substantial effect on the cross-relaxation rates, changing the ratio $\sigma_L/\sigma_R$ from about 0.5 to 0 (at 600 MHz). The value of the cutoff radius is critical: By changing it from 4 to 8 Å, say, we increase the excluded volume by a factor 8. For the protein BPTI, which has served as testing ground for intermolecular NOE studies,[9,10] 97% of all macromolecular protons are within 8 Å of one or more protons in side-chain hydroxyl, ammonium or guanidinium groups or in one of the four buried water molecules. Figure 12 shows the combined effect of the distance of closest approach, $d$, for the mobile $S$ spins, and of the number and distance of long-lived $S$ spins. For $d = 3-5$ Å, the mobile $S$ spins yield $\sigma_L/\sigma_R$ values in the range 0.2–0.5. However, when the effect of a few long-lived $S$ spins is included, $\sigma_L/\sigma_R$ becomes negative and may even approach the slow-motion limit of $-1/2$.

The ratio $\sigma_L/\sigma_R$ is often used as a residence time indicator for water molecules interacting with biomolecules.[9–12] For a Lorentzian SDF, the zero-crossing of $\sigma_L$ occurs at a correlation time $\tau_C = \sqrt{5}/(4\pi\nu_0)$, which equals 0.30 ns at a Larmor frequency of 600 MHz. If $\tau_R$ is much longer, Eq. (3.6) shows that $\tau_C$ may be identified with the residence time $\tau_M$. This intramolecular case corresponds to the dashed–dotted curve in Fig. 13. Note that this curve does not depend on the number $N_M$ of site-bound $S$ spins or on their distance

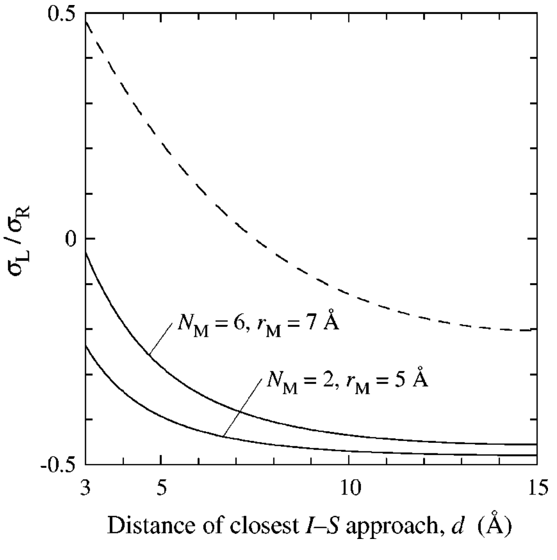

FIG. 12. Ratio of the homonuclear laboratory-frame ($\sigma_L$) and rotating-frame ($\sigma_R$) cross-relaxation rates vs the distance of closest approach $d$. Unrestricted nonuniform diffusion in the presence of two long-lived $S$ spins at $r_M = 5$ Å or 6 long-lived $S$ spins at $r_M = 7$ Å. Parameter values from Table I. The dashed curve is obtained in the absence of long-lived $S$ spins.

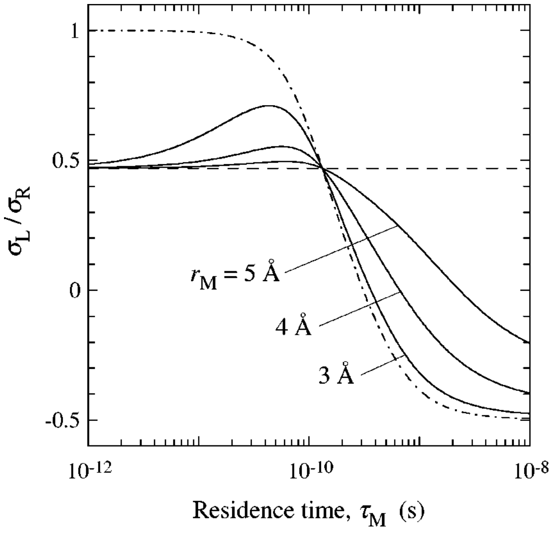

FIG. 13. Ratio of the homonuclear laboratory-frame ($\sigma_L$) and rotating-frame ($\sigma_R$) cross-relaxation rates vs the residence time $\tau_M$ of two $S$ spins at a distance $r_M = 3$, 4 or 5 Å from the $I$ spin. Unrestricted nonuniform diffusion with parameter values from Table I, but $D_T^{(0)}/D_T^{(1)} = 2$. The dashed line is obtained in the absence of long-lived $S$ spins and the dashed–dotted curve with only the long-lived $S$ spins.

$r_M$ from the $I$ spin. In the absence of such site-bound $S$ spins, the mobile $S$ spins yield $\sigma_L/\sigma_R = 0.47$ (the dashed line in Fig. 13) for $D_T^{(0)}/D_T^{(1)} = 2$, which is a plausible value when water molecules in deep surface pockets are excluded,[17,18] i.e., the water molecules with residence time $\tau_M$ that are treated explicitly in Fig. 13.

The three solid curves in Fig. 13 show how $\sigma_L/\sigma_R$ depends on the residence time $\tau_M$ and distance $r_M$ of a single relatively long-lived water molecule in the presence of the mobile $S$ spins. These curves must fall between the two limiting cases, represented by the dashed horizontal line and the dashed–dotted Lorentzian curve. With increasing residence time $\tau_M$, $\sigma_L/\sigma_R$ goes from the former to the latter limit. As a consequence, $\sigma_L/\sigma_R$ increases with $\tau_M$ below about 0.1 ns. This behavior contradicts the widespread notion that slower hydration dynamics corresponds to smaller $\sigma_L/\sigma_R$, which is not generally true. Figure 13 shows that a single water molecule affects $\sigma_L/\sigma_R$ significantly only if its residence time is longer than about 0.2 ns. Furthermore, the zero-crossing depends strongly on the distance of this water molecule from the $I$ spin, increasing by an order of magnitude when $r_M$ goes from 3 to 5 Å. Finally, we note that the results in Fig. 13 are valid only in the absence of contributions from long-lived ($\tau_M \gg \tau_R$) $S$ spins. As noted above, this is an unlikely situation.

## IV. DISCUSSION

During the past 15 years, biomolecular hydration has been thoroughly investigated by two different NMR techniques: magnetic relaxation dispersion (MRD) of the quadrupolar $^2$H and $^{17}$O nuclides in the water molecule[20,21] and intermolecular $^1$H–$^1$H NOEs.[11,12] Neither method can separate hydration water from bulk water in the NMR spectrum because fast water exchange makes the water ($^1$H, $^2$H or $^{17}$O) resonance degenerate. Nevertheless, different classes of water molecules can be identified and characterized. In the MRD method, a dynamic selection is accomplished by exploiting the fact that water molecules with different rotational correlation times give rise to characteristic frequency dependencies (dispersions) in the longitudinal relaxation rate.[20,21] In the NOE method, the selection is more complicated, being dependent on both the mobility and proximity of water molecules to protein protons with resolved $^1$H resonances. While the MRD and NOE methods are well-established and complementary tools for identifying and characterizing internal water molecules buried inside proteins, their application to the study of surface hydration presents experimental challenges as well as theoretical problems. The present theoretical analysis of intermolecular dipolar cross-relaxation between macromolecular and solvent spins has important implications for NOE studies of biomolecular hydration. Rather than attempting a detailed reassessment of published NOE data (to appear elsewhere), we conclude with some general observations.

The crucial point made here is that intermolecular NOEs to solvent spins are of long range. NOEs involving the solvent-exposed protons at the macromolecular surface therefore tend to be dominated by long-range dipole couplings to a very large number of water molecules in the bulk solvent region. As a consequence, NOEs can provide little or no information about the vast majority of water molecules interacting with the macromolecular surface. In the past, NOE data on surface hydration have been interpreted in terms of variants of the intramolecular model or in terms of the uniform diffusion model.[5] These models are inappropriate; the former because they ignore the dominant long-range contribution and the latter because it assigns the same diffusion coefficient to all water molecules in the system.

In the usual analysis of intermolecular NOEs with the aid of the uniform diffusion model,[9–12] the ratio $\sigma_L/\sigma_R$ is converted to a water diffusion coefficient by means of a sigmoidal curve like that in Fig. 14. For example, with the parameter values used in Fig. 14, $\sigma_L/\sigma_R = 0.2$ corresponds, according to the uniform diffusion model, to a diffusion coefficient $D_T = 0.83 \times 10^{-9}$ m$^2$ s$^{-1}$. However, this value pertains to all water molecules and therefore cannot serve as a measure of hydration dynamics. For the same $\sigma_L/\sigma_R$ value, the nonuniform model yields $D_T^{(1)} = 0.10 \times 10^{-9}$ m$^2$ s$^{-1}$. This corresponds to a retardation factor of 20, an order of magnitude more than expected for exposed surface sites.[17,18] For exposed surface protons of the small protein BPTI, $\sigma_L/\sigma_R$ values in the range 0.1–1.0 have been reported.[22] In contrast, with retardation factors derived from MRD data, the nonuniform diffusion model predicts that $\sigma_L/\sigma_R$ should lie in the range 0.4–0.5 for exposed surface protons. In particular, $\sigma_L/\sigma_R$ values close to 1, as reported for many surface protons in BPTI,[22] cannot be rationalized by the diffusion model because dipole couplings to remote bulk water molecules are modulated slowly, not because the water molecules diffuse slowly, but because they have to move a large distance to randomize the orientation of the internuclear vector. As discussed elsewhere, such large $\sigma_L/\sigma_R$ values are likely to be experimental artifacts. On the other hand, most

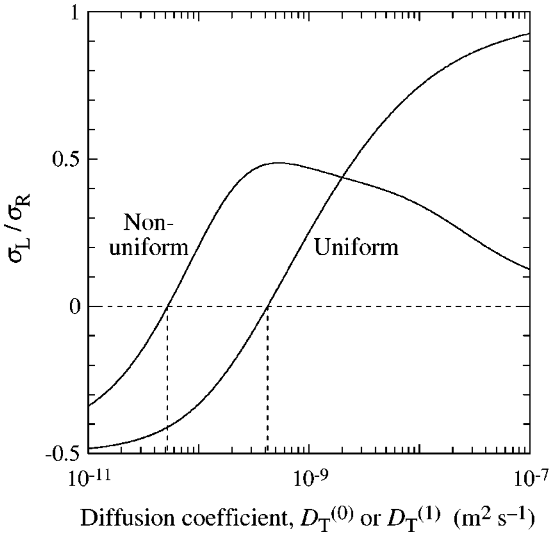

FIG. 14. Ratio of the homonuclear laboratory-frame ($\sigma_L$) and rotating-frame ($\sigma_R$) cross-relaxation rates vs the translational diffusion coefficient $D_T^{(0)}$ (uniform diffusion) or $D_T^{(1)}$ (nonuniform diffusion). Unrestricted uniform or nonuniform diffusion with parameter values from Table I. The dashed lines indicate the zero-crossing of $\sigma_L / \sigma_R$.

of the small $\sigma_L / \sigma_R$ values appear to result from intramolecular NOEs to rapidly exchanging labile protein protons. Such artifacts are usually deemed insignificant if the observed protein proton is more than 4–5 Å from any rapidly exchanging labile proton.[10,12] However, as shown in the foregoing, more remote labile protons can make substantial contributions to the weak NOEs observed with surface protons.

The nonmonotonic variation of $\sigma_L / \sigma_R$ as a function of water mobility or residence time, predicted by the nonuniform diffusion model, demonstrates that this ratio cannot be used as an indicator of hydration dynamics. As illustrated by Fig. 14, an increase of $\sigma_L / \sigma_R$ can result from either decreased or increased hydration water mobility. Accordingly, $\sigma_L / \sigma_R$ is not a single-valued function of $D_T^{(1)}$ and this ambiguity appears in the experimentally most relevant region (retardation factor 1–4). The maximum in $\sigma_L / \sigma_R$ results from two opposed effects of increased hydration water mobility. When $D_T^{(1)} \ll D_T^{(0)}$ (large retardation), water molecules in the hydration layer make large contributions to both $\sigma_L$ and $\sigma_R$ and the ratio increases with $D_T^{(1)}$ in the same sigmoidal way as for the uniform model. For sufficiently large retardation, $\sigma_L / \sigma_R$ attains the same limit, $-1/2$, as in the uniform case. As $D_T^{(1)}$ increases, the relative contribution from hydration water to $\sigma_L$ and $\sigma_R$ decreases and the contribution from bulk water becomes increasingly important. Even while $D_T^{(1)}$ remains smaller than $D_T^{(0)}$ (between the maximum and crossover in Fig. 14), $\sigma_L / \sigma_R$ passes through a maximum and then decreases as the relative contribution from the more mobile bulk water molecules increases further. This happens because the characteristic time scale for modulation of the orientation of the internuclear vector is longer for the more remote (albeit more mobile) bulk water molecules. In the (physically implausible) limit $D_T^{(1)} \gg D_T^{(0)}$, the hydration water contribution is negligible and $\sigma_L / \sigma_R$ levels out at a value (0.044 for the parameter values used in Fig. 14) that corresponds roughly to a larger macromolecule (radius $b + \delta$) surrounded by bulk water. (The correspondence is not exact because the hydration layer also acts as a ‘‘correlation sink’’ for nearby bulk water molecules.)

Results on surface hydration dynamics obtained by the NOE and MRD methods have not previously been compared directly because of the incompatible models used to interpret NOE and MRD data. However, the nonuniform diffusion model allows contact to be made between the two methods. MRD data yield the quantity $N_{\mathrm{hyd}}(\tau_R^{(1)}/\tau_R^{(0)} - 1)$, where $\tau_R^{(1)}$ is the rotational correlation time of the $N_{\mathrm{hyd}}$ water molecules in the hydration layer and $\tau_R^{(0)}$ is the (known) rotational correlation time of bulk water.[20,21] Because both translational and rotational motions of water molecules are rate-limited by the underlying hydrogen bond dynamics, the rotational retardation factor $\tau_R^{(1)}/\tau_R^{(0)}$ can be identified with the translational retardation factor $D_T^{(0)}/D_T^{(1)}$. Furthermore, the number $N_{\mathrm{hyd}}$ of retarded water molecules can be related to the hydration layer thickness $\delta$ by means of Eq. (3.4). When MRD results are used to predict NOE results in this way, one finds that the modest slowing down of water motions in the hydration layer has a negligible effect on the $\sigma_L / \sigma_R$ ratio.

In the past, NOE results have invariably been discussed in terms of model-dependent water residence times rather than the more robust retardation factors. To be consistent with the nonuniform diffusion model, the water residence time should be defined as the mean time taken for a water molecule to reach the outer boundary of the hydration layer (at $r = b + \delta$) with its initial position uniformly distributed within the hydration layer ($b < r < b + \delta$). This so-called mean-first-passage-time can be obtained by direct integration of the diffusion equation, subject to reflection and absorption boundary conditions at $r = b$ and $r = b + \delta$, respectively. The result is[23]

$$\tau_{\mathrm{res}} = \frac{\delta^2}{3 D_T^{(1)}} \left[ 1 - \frac{\delta}{b} + \mathcal{O}\left( \frac{\delta^2}{b^2} \right) \right]. \tag{4.1}$$

With a retardation factor of 2 (Refs. 17, 18) and $\delta = 3$ Å $\ll b$, this yields $\tau_{\mathrm{res}} = 30$ ps at 25 °C.

The water–protein $^1$H–$^1$H NOE method has a precedent in the closely analogous experiment where a nitroxide spin label is covalently attached to the protein to probe the mobility of hydration water via the longitudinal $^1$H relaxation rate $R_1^I$ induced by the intermolecular dipole–dipole coupling between the water proton and the unpaired electron spin.[24,25] In this case,[1]

$$R_1^I = K_{IS} [0.1\, J^{(2)}(\omega_I - \omega_S) + 0.3\, J^{(2)}(\omega_I) + 0.6\, J^{(2)}(\omega_I + \omega_S)], \tag{4.2}$$

where $\omega_I$ and $\omega_S$ are the angular Larmor frequencies of the proton and electron, respectively. To estimate the spatial extent of the aqueous region probed by this experiment, $R_1^I$ was calculated as described in Sec. II D (uniform model) but with the upper integration limits in Eq. (2.17) replaced by $c$.[24] By this simpe device one restricts the initial and final positions of the $S$ spin to the region $b < r < c$ but, since the infinite-space propagator is retained, one does not exclude diffusive trajectories that sample the region $r > c$ at intermediate times.

Such trajectories are excluded by imposing an absorbing boundary at $r = c$, as in our calculations (Sec. II E). In either case, one finds that the spin-label experiment has a much shorter range than the intermolecular NOE experiment, with $R_1^I$ converging to 90% at $\delta = c - b = 10$ Å and to 80% at 5 Å.[24] This difference is mainly due to the large magnetic moment of the electron, which of course does not affect the $r^{-6}$ dependence of the individual dipole–dipole couplings, but makes $\omega_S = 658\omega_I$. As a result, $R_1^I$ probes water motions at much higher frequency than the homonuclear cross-relaxation rates, which involve the zero-frequency SDF $J^{(2)}(0)$.

## ACKNOWLEDGMENT

This work was supported by the Swedish Research Council.

## APPENDIX: TRANSLATION-ROTATION DECOUPLING IN THE INTERMOLECULAR TCF

The essential step in our derivation of Eq. (2.5) is a one-center expansion of the solid harmonic $F_{2,0}(\mathbf{R} - \boldsymbol{\rho})$ about the center of the *I* sphere (see Fig. 1). This expansion, based on a rotational transformation of the spherical harmonic $Y_{2,0}(\Omega)$ and a Laplace-type expansion of $r^{-3}$, takes the form[26]

$$F_{2,0}(\mathbf{R} - \boldsymbol{\rho}) = \sum_{L=0}^{\infty} \sum_{M=-L}^{L} A_{LM} \rho^L Y_{L,-M}(\Omega^{\boldsymbol{\rho}}) F_{L+2,M}(\mathbf{R}). \tag{A1}$$

Here, $\Omega^{\boldsymbol{\rho}}$ denotes the spherical polar angles that specify the orientation of the vector $\boldsymbol{\rho}$ in the laboratory-fixed frame. Furthermore,

$$A_{LM} = (-1)^L \left( \frac{10\pi}{3} \right)^{1/2} [(L+1)(L+2)(2L+3)]^{1/2} \times \begin{pmatrix} L & 2 & L+2 \\ -M & 0 & M \end{pmatrix}. \tag{A2}$$

The purpose of the expansion (A1) is to factorize the dependence on the vectors $\mathbf{R}$ and $\boldsymbol{\rho}$. If the translational motion modulating $\mathbf{R}$ and the rotational motion modulating $\boldsymbol{\rho}$ are statistically independent, the total TCF $g^{(2)}(\tau)$ can be expressed as a sum of products of partial TCFs,

$$\begin{aligned} g^{(2)}(\tau) &\equiv \langle F_{2,0}(\mathbf{R}_0 - \boldsymbol{\rho}_0) F_{2,0}(\mathbf{R} - \boldsymbol{\rho}) \rangle \\ &= \sum_{L=0}^{\infty} \sum_{L'=0}^{\infty} \sum_{M=-L}^{L} \sum_{M'=-L'}^{L'} A_{LM} A_{L'M'} \\ &\quad \times \langle \rho_0^L Y_{L,-M}^*(\Omega_0^{\boldsymbol{\rho}}) \rho^{L'} Y_{L',-M'}(\Omega^{\boldsymbol{\rho}}) \rangle \\ &\quad \times \langle F_{L+2,M}^*(\mathbf{R}_0) F_{L'+2,M'}(\mathbf{R}) \rangle. \end{aligned} \tag{A3}$$

If the vector $\boldsymbol{\rho}$ is of fixed length and undergoes isotropic rotational diffusion, then

$$\langle \rho_0^L Y_{L,-M}^*(\Omega_0^{\boldsymbol{\rho}}) \rho^{L'} Y_{L',-M'}(\Omega^{\boldsymbol{\rho}}) \rangle = \delta_{LL'} \delta_{MM'} \rho^{2L} G_R^{(L)}(\tau) \tag{A4}$$

with the purely rotational TCF,

$$G_R^{(L)}(\tau) = (4\pi)^{-1} \exp[-L(L+1) D_R \tau]. \tag{A5}$$

Combination of Eqs. (A3) and (A4) yields

$$g^{(2)}(\tau) = \sum_{L=0}^{\infty} \sum_{M=-L}^{L} A_{LM}^2 \rho^{2L} G_R^{(L)}(\tau) \times \langle F_{L+2,M}^*(\mathbf{R}_0) F_{L+2,M}(\mathbf{R}) \rangle. \tag{A6}$$

The last factor is a purely translational TCF and, on account of the cylindrical symmetry about $\mathbf{R}$, it cannot depend on the index *M*. We can therefore set $M = 0$. The sum over *M* in Eq. (A6) then only involves the $3 - j$ symbol in Eq. (A2). Using the orthogonality relation[13]

$$\sum_{M=-L}^{L} \begin{pmatrix} L & 2 & L+2 \\ -M & 0 & M \end{pmatrix}^2 = \frac{1}{5} \tag{A7}$$

we thus obtain

$$g^{(2)}(\tau) = \frac{2\pi}{3} \sum_{L=0}^{\infty} (L+1)(L+2)(2L+3) \rho^{2L} G_R^{(L)}(\tau) \times \langle F_{L+2,0}(\mathbf{R}_0) F_{L+2,0}(\mathbf{R}) \rangle. \tag{A8}$$

Multiplying by $4\pi N_S$ and using the definition (2.4), we arrive at the desired Eq. (2.5). A different derivation of this result has been presented by Ayant *et al.*[5]

If rotation is much faster than translation, then the total TCF in Eq. (A3) can be decomposed as

$$g^{(2)}(\tau) = g_R(\tau) + \langle F_{2,0}(\mathbf{R}_0) F_{2,0}(\mathbf{R}) \rangle, \tag{A9}$$

where the last term is the purely translational TCF obtained with a centered *I* spin. In the SDF, the rotational TCF $g_R(\tau)$ contributes significantly only at frequencies above the translational dispersion. The second term in Eq. (A9) is obtained by noting that, on time scales $\tau$ where the first term has practically decayed to zero, the rotational TCFs in Eq. (A3) can be replaced by the corresponding product of isotropic equilibrium averages. For a $\boldsymbol{\rho}$ vector of fixed length, we then have

$$\begin{aligned} &\langle Y_{L,-M}^*(\Omega_0^{\boldsymbol{\rho}}) Y_{L',-M'}(\Omega^{\boldsymbol{\rho}}) \rangle \\ &\quad = \langle Y_{L,-M}^*(\Omega_0^{\boldsymbol{\rho}}) \rangle \langle Y_{L',-M'}(\Omega^{\boldsymbol{\rho}}) \rangle \\ &\quad = \delta_{L0} \delta_{L'0} \delta_{M0} \delta_{M'0} \frac{1}{4\pi}. \end{aligned} \tag{A10}$$

By inserting this into Eq. (A3) and noting that $A_{00} = (4\pi)^{1/2}$, we obtain the second term in Eq. (A9).

With the aid of a two-center expansion of the solid harmonics,[26] it is straightforward to generalize Eq. (A9) to the case where both spin *I* and *S* are located off-center.[5] In the same way as we have done for the *I* spin, it can be shown that the off-center location of the *S* spin only affects the total TCF on the short time scale of solvent rotation.

[1] A. Abragam, *The Principles of Nuclear Magnetism* (Clarendon, Oxford, 1961).

[2] H. C. Torrey, Phys. Rev. **92**, 962 (1953).

[3] L.-P. Hwang and J. H. Freed, J. Chem. Phys. **63**, 4017 (1975).

[4] Y. Ayant, E. Belorizky, J. Alizon, and J. Gallice, J. Phys. (Paris) **36**, 991 (1975).

[5] Y. Ayant, E. Belorizky, P. Fries, and J. Rosset, J. Phys. (Paris) **38**, 325 (1977).

[6] P. S. Hubbard, Phys. Rev. **131**, 275 (1963).

[7] J. F. Harmon and B. H. Muller, Phys. Rev. **182**, 400 (1969).

[8] P. H. Fries and G. N. Patey, J. Chem. Phys. **80**, 6253 (1984).

[9] G. Otting, E. Liepinsh, and K. Wüthrich, Science **254**, 974 (1991).

[10] K. Wüthrich, G. Otting, and E. Liepinsh, Faraday Discuss. **93**, 35 (1992).

[11] G. Otting and E. Liepinsh, Acc. Chem. Res. **28**, 171 (1995).

[12] G. Otting, Prog. Nucl. Magn. Reson. Spectrosc. **31**, 259 (1997).

[13] D. M. Brink and G. R. Satchler, *Angular Momentum*, 2nd ed. (Clarendon, Oxford, 1968).

[14] B. Halle, Mol. Phys. **60**, 319 (1987).

[15] B. Halle, J. Chem. Phys. **94**, 3150 (1991).

[16] D. Neuhaus and M. P. Williamson, *The Nuclear Overhauser Effect in Structural and Conformational Analysis*, 2nd ed. (Wiley–VCH, New York, 2000).

[17] B. Halle, in *Hydration Processes in Biology*, edited by M.-C. Bellisent-Funel (IOS, Amsterdam, 1999), pp. 233–249.

[18] B. Halle and M. Davidovic, Proc. Natl. Acad. Sci. USA **100**, 12135 (2003).

[19] R. Brüschweiler and P. E. Wright, Chem. Phys. Lett. **229**, 75 (1994).

[20] B. Halle, V. P. Denisov, and K. Venu, in *Biological Magnetic Resonance*, edited by N. R. Krishna and L. J. Berliner (Kluwer Academic/Plenum, New York, 1999), Vol. 17, pp. 419–484.

[21] B. Halle and V. P. Denisov, Methods Enzymol. **338**, 178 (2001).

[22] R. M. Brunne, E. Liepinsh, G. Otting, K. Wüthrich, and W. F. van Gunsteren, J. Mol. Biol. **231**, 1040 (1993).

[23] D. Y. C. Chan and B. Halle, Biophys. J. **46**, 387 (1984).

[24] C. F. Polnaszek and R. G. Bryant, J. Chem. Phys. **81**, 4038 (1984).

[25] H.-J. Steinhoff, B. Kramm, G. Hess, C. Owerdieck, and A. Redhardt, Biophys. J. **65**, 1486 (1993).

[26] Y.-N. Chiu, J. Math. Phys. **5**, 283 (1964).